Research Square

Preprints are preliminary reports that have not undergone peer review.
They should not be considered conclusive, used to inform clinical practice,
or referenced by the media as validated information.

GDL-free multi-phase flow reactors enable stable intermittent CO2 electrolysis

Magda Helena Barecka

m.barecka@northeastern.edu

Northeastern University https://orcid.org/0000-0002-0772-164X

Max Moran

Northeastern University https://orcid.org/0009-0003-5063-0043

Article

Keywords:

Posted Date: November 19th, 2026

DOI: https://doi.org/10.21203/rs.3.rs-11764088/v1

License: This work is licensed under a Creative Commons Attribution 4.0 International License.
Read Full License

Additional Declarations: Yes there is potential Competing Interest. The authors are inventors listed on a non-provisional patent application PCT/US2025/036944 for multiphase flow reactors. MHB is a part of the Advisory board of iScience and Chem Circularity. There are no other conflicts of interest to disclose.

GDL-free multi-phase flow reactors enable stable intermittent CO_2 electrolysis

Max Moran[1], Magda H. Barecka*[1,2]
[1]Department of Chemical Engineering, Northeastern University, 360 Huntington Avenue, Boston, MA, USA
[2]Department of Chemistry and Chemical Biology, Northeastern University, 360 Huntington Avenue, Boston, MA, USA
*corresponding author, m.barecka@northeastern.edu

Abstract

Gas diffusion electrodes (GDE) offer an excellent interface for intensifying mass transfer for fundamental investigations and industrial CO_2 electroreduction; however, the operational GDE stability remains a major limitation. GDE flooding, salt precipitation, and catalyst restructuring can worsen under intermittent renewable operation. Here we present a multi-phase flow reactor that controls the reaction microenvironment through flow regimes and eliminates the need for a GDE. Using an optically accessible cell and operando bubble tracking, we studied slug and annular flow over silver for CO_2-to-CO conversion. Both flows enhance CO_2 transport over single-phase flow (~2x and ~3x peak iCO). We identified boundary-layer renewal, not film thickness, as the governing mechanism, establishing flow velocity and renewal rate as key design levers. The reactor tolerates repeated shutdown and restart, recovering voltage and FE with minimal reconditioning across five days. This study establishes multi-phase flow as a stable flow architecture with guiding design principles for intermittent CO_2 electroreduction.

Introduction

As CO_2 emissions reach new annual highs, large-scale carbon capture, utilization, and storage (CCUS) will be required to meet international climate goals[1][2]. Current industrial CCUS has yet to achieve significant removal rates, and there is a growing need for novel CCUS techniques. With renewable energy becoming less expensive and more available, especially during the peak periods of intermittent production, electrochemical CO_2 reduction reaction (CO2RR) has emerged as a promising alternative for converting CO_2 into value-added products, such as syngas, methane, and ethylene[3][4]. Besides potential positive environmental impacts, CO2RR can also help to address the vulnerability of the chemical supply chain to potential disruptions in, e.g., oil supply, offering a pathway to more resilient, distributed manufacturing. Yet, to achieve this impact, the CO2RR field needs not only to demonstrate industrially relevant performance metrics, but also the

ability to integrate within the energy ecosystem and to operate flexibly when surplus electricity is available.

Viability of CO2RR requires low cell overpotential, high current density (>100 mA/cm^2), high product faradaic efficiency (FE), and long-term stability (>20,000 hours)[5][6][7]. It remains challenging to demonstrate all these metrics simultaneously, and intermittent operation creates further stability complications[8]. The stability of intermittently operating reactors is critical to address, since such reactors can take advantage of dynamic electricity pricing[9][10], operate only when energy cost is low, improving the overall techno-economics of the CO2RR process. While CO2RR catalysts govern reaction selectivity, mass transport-related phenomena can determine the reaction outcome and are critical to the operational stability. Out of multiple mass transport mechanisms pertinent to electrochemical systems, CO_2 diffusion to the catalyst is often the rate-limiting step and governs both overpotential and achievable current density[11].

Current industrial designs utilize gas diffusion electrodes (GDEs) and membrane electrode assemblies (MEAs) to shorten CO_2 diffusion paths utilizing a gas diffusion layer (GDL, Fig. 1a), which enables high current densities above 100 mA/cm^2 and, in some cases,>1 A/cm^2[12][13][14]. GDLs consist of carbon- or polymer-based microporous structures, frequently treated for enhanced hydrophobicity. The structural and chemical complexity of GDL architectures makes them prone to failure modes that reduce long-term stability, including electrolyte flooding, salt precipitation[1][13][15], catalyst restructuring[11][16][17][18], and GDL rupture[13]. Despite great progress in mitigating failure modes[19][20][21][22], these drawbacks motivated us to seek reactor designs that retain GDEs/MEAs transport enhancement while avoiding stability concerns.

Multi-phase microreactors offer a potential solution with enhanced transport and scalability[23][25]. Multi-phase flow consists of simultaneous gas-liquid flow, which can form various regimes depending on flow conditions. Regimes with consistent flow behavior, such as Taylor (slug) and annular flow (Fig. 1b), provide a more predictable environment for reaction. In slug flow, gas bubbles fill most of the channel and alternate with liquid slugs, which are connected by a thin liquid film between the gas and wall. Recirculating vortices in the liquid slugs enhance the mass transport from the slug to the wall and from the bubble caps to the slug[23][24][25], and the thin liquid film allows rapid saturation of gas phase reactants[26]. These enhancements have been shown to improve reactor performance in monolith reactors[25][26][27] and photochemical applications[28]. In annular flow, the liquid slugs are absent, and a continuous gas-phase core is separated from the wall by a thin, wavy liquid film[25]. Compared to Taylor flow, annular flow has only one mass transfer pathway isolated to the film surrounding the gas.

Importantly, controlling the multiphase flow through physical flow structures and their respective transport pathway(s) can enable tuning of the thin electrolyte film and

shortening of the diffusion path to a micrometer range (similar to what was reported in GDE/MEA reactors), yet the porous, hydrophobic layer is no longer needed, opening an opportunity for a GDL-free operation. By enabling insights into catalyst performance unaffected by crystallization, flooding, or GDL degradation, such reactor designs can be both impactful for fundamental catalytic studies and large-scale CO2RR applications.

While the theoretical insights into multiphase flow suggest a promising new interface for electrochemical reactions, few studies have operated electrochemical Taylor slug flow, and results have been mixed. *Cao et al.* studied the electrocatalytic hydrogenation of furfural under Taylor flow between two electrodes and found that the thin liquid film dominated the enhanced mass transfer but also created a region of very high resistance that increased overpotential[26]. *Zhang et al.* reported the first slug-flow CO_2 reduction studies on silver and copper, achieving higher carbon product FEs than an h-cell up to 20 mA/cm^2[29][30]. *Bagemihl et al.* modeled CO2RR under Taylor flow in a tubular reactor and predicted an order of magnitude increase in limiting current density over an h-cell, exceeding 100 mA/cm^2[31]. In the model, the film dominated mass transfer at low velocities, while at higher velocities, the film thickened and total current dropped. Higher void fractions lengthened the film region and improved both current and FE[31]. *Bagemihl* also developed an experimental rectangular channel cell with a silver cathode, which improved CO selectivity over single-phase flow but was outperformed by an H-cell[32]. Contrary to the tubular model, the gas-liquid ratio had little effect, and higher velocity improved performance, suggesting that the dominant mass-transfer pathway is the slug rather than the film because the slug has a thinner diffusive boundary layer. However, no firm conclusion could be drawn due to the difficulties in quantifying the underlying phenomena, including film thickness and corner flow, and further flow regimes were not examined. Annular flow has been extensively studied for gas-liquid mass transfer properties[33][34][35], but it has received little attention in electrochemistry, particularly CO2RR.

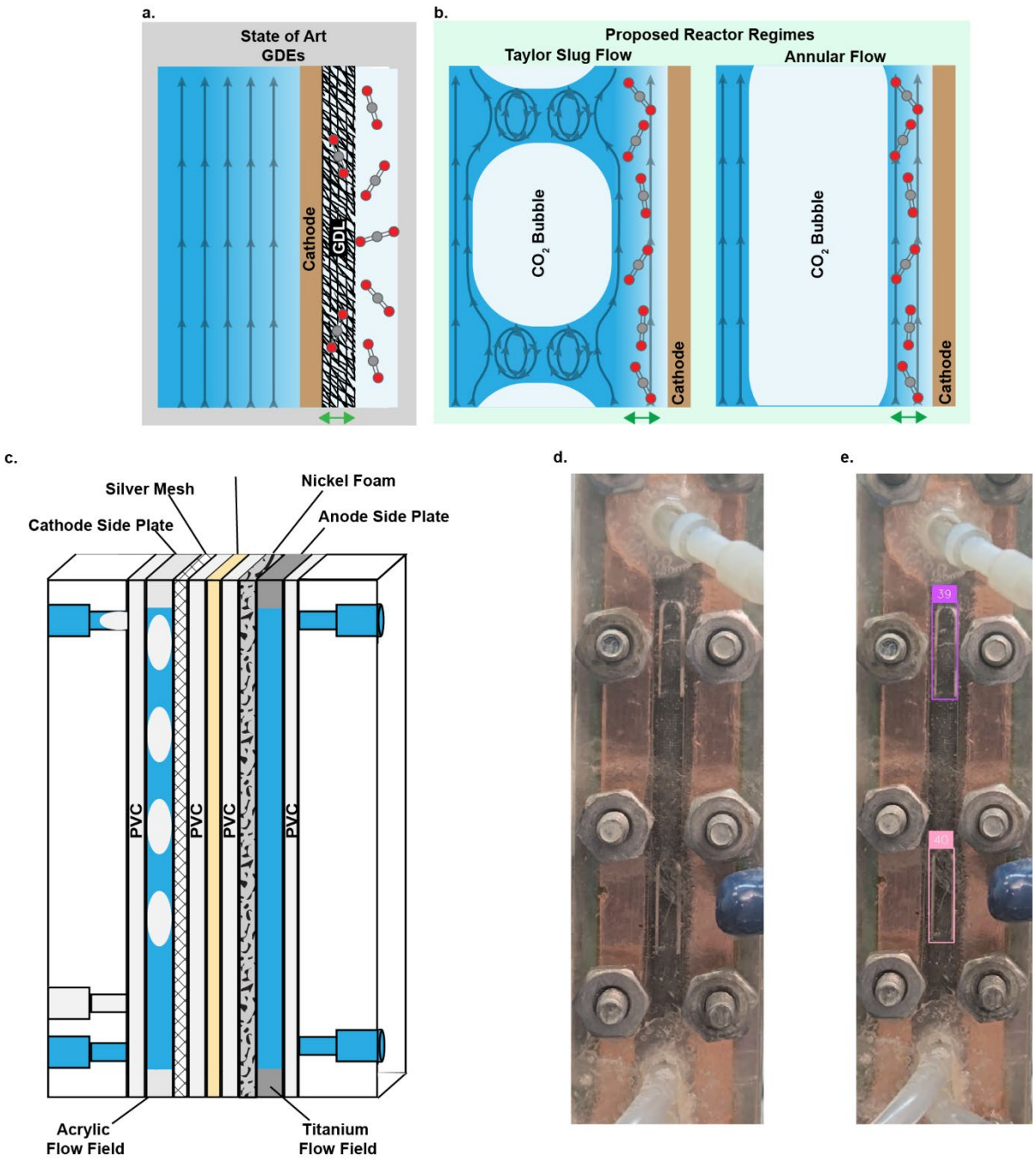
In this Article, we study how multi-phase flow regimes (Taylor and annular) affect mass transport and CO2RR performance, demonstrating how to leverage this interface for a GDL-free operation. Starting with Taylor flow, we develop an imaging-accessible reactor and an Artificial Intelligence (AI)-based operando bubble-tracking pipeline to quantify the real flow conditions and evaluate the governing dimensionless numbers. We show that, over a silver mesh cathode, slug flow enhances CO2RR performance relative to single-phase liquid flow, and both gas-liquid ratio and velocity influence selectivity and mass-transport-limited partial current density. We then access gravity-driven annular film flow through orientation change, which raises the transport-limited current density further. Because annular flow has no liquid slugs, its enhancement with velocity isolates the film diffusive boundary layer as its enhancement pathway. Across both regimes over a silver catalyst, we identify convective renewal and the thinning of the diffusion boundary layer,

not film thickness, as the governing mechanism, establishing boundary-layer renewal as the relevant design lever. Finally, we address the practical application of the reactor and apply anode modifications that improve efficiency without compromising cathode selectivity. We assess stability relevant to operation under intermittent power sources, demonstrating stable Faradaic Efficiency and full cell potential over a series of shutdowns with no conditioning, cleaning, or protective potential applied. The collective importance of performance metrics reported in this paper is analyzed through a techno-economic study, showing that intermittently powered multiphase-flow reactors can allow us to convert CO_2 to syngas at a price less than its current market price, as long as they operate min. 1000 hours per year. Our results establish multi-phase flow as a transport enhancement strategy for CO_2 electroreduction and provide mechanistic design principles for advancing multi-phase CO2RR reactors for both fundamental, GDL-free catalytic studies and large-scale application toward industrially relevant performance.

Results and Discussion

Reactor testing and flow analysis

We designed an imaging accessible, transparent single-channel flow reactor inspired by *Bagemihl*[32] (Fig. 1c), featuring laser-cut acrylic inlet plates. In contrast to the previously reported design, we implemented rectangular instead of square channels, as this allowed us to increase the width (to ensure better membrane exposure and thus sufficient ionic transport) and to reduce the height of the channel (to minimize overpotential and improve the energy efficiency). The acrylic cathode flow plate generates slug flow with two inlets (Fig. 1d and Methods section). Note that the slug flow is formed on one side of the cathode, and the membrane and anode are situated on the other side of the cathode; therefore, slug flow should not contribute to an increased overpotential. We utilize rectangular flow channels due to ease of scaling and the well-studied transport behaviors that allow us to leverage previous design principles established for sandwich-type hydrogen electrolyzers[36][37]. We began our study by analyzing slug flow, as a more studied and observable regime. To establish a qualitative understanding of the flow formation, we recorded a video of each test to develop an operando bubble tracking pipeline using a YOLOv8n object detection model trained via Roboflow. This model identifies gas bubbles from the visible gas-liquid interface, allowing us to extract flow information, such as bubble speed and bubble/slug length, directly from recordings (Fig. 1e; see Methods section and Supplementary Note 1 for more detailed algorithm information and validation). This tracking approach applies only to slug flow with discrete gas bubbles; the annular regime will require different analysis methods.



151

152 **Figure 1: Multiphase flow reactors for electrochemical CO_2 conversion. a,**
153 Schematic of the flow structure in a flow cell with GDE. **b,** Schematics of the flow
154 structures in the proposed Taylor slug regime and annular regime. **c,** Schematic
155 illustration of the multi-phase flow reactor construction with an example multi-phase slug
156 flow. **d,** Image of multi-phase slug flow in assembled reactor. **e,** Image output of flow
157 analysis algorithm with bounding boxes automatically assigned to gas bubbles.

158

The gas bubble velocities and length govern mass transport in the reactor, and dimensionless numbers describe the balance of different forces within the flow. Most depend on the two-phase velocity, U:

$$U = \frac{Q_g + Q_l}{A}$$

$$Q_g = L_B * f * A$$

where Q_G and Q_L are the gas and liquid volumetric flow rates, A is the channel cross-sectional area, L_B is the bubble length, and f is the bubble frequency.

To understand flow formation, we first analyzed gas bubble data from 14 repetitions of the same experiment with no applied current (Table 1). Typically, the bubble data speed/length is calculated based on mass flow controllers setpoints, yet our approach allowed us to compare it to the actual velocities achieved in each test. Interestingly, video data differs from setpoint-based calculations, highlighting that CO2RR multiphase flow performance should be studied under real flow conditions rather than inlet setpoints. Moreover, we found that minor differences in the reactor assembly can produce significantly different flow characteristics (see min/max outliers). Therefore, we also used video data as an additional tool to verify the reproducibility of the achieved flow conditions and ensure that the enhancement in CO2RR performance stems from the studied flow regime, not other factors.

With access to operando bubble data, we calculated dimensionless numbers to further characterize flow formation. The Reynolds number (inertial vs. viscous forces) is used to map flow regimes[38][39]. Our low values confirm a laminar flow regime. The Capillary number (viscous vs. surface tension forces) appears in many film-thickness correlations[38][39]. Our low Ca indicates that surface tension dominates, so bubbles will not be axisymmetric and will flatten against the channel walls[25]. Because Ca depends on bubble velocity, its variance may affect film mass-transport pathways and contribute to performance differences. The Froude Number (inertial vs gravitational forces) indicates the role of gravity, especially in millimeter-scale channels[38]. Our very low Fr signals that gravity is significant at our velocities. As Fr decreases, gravity thickens the film, and this effect is more significant in square channels and with upward flow[25][40]. Finally, the Bond number (gravitational vs. surface tension forces) classifies the flow regime, with a critical Bo of <4.7 indicating slug flow rather than stratified flow formation[25][38][39]. Our Bo confirms that gravity does not disrupt slug flow formation but can still play a role in the film thickness[25][39][41]. Collectively, these results suggest the formation of the desired laminar, non-stratified slug flow and indicate that gravity is an important factor to further investigate.

Table 1: Comparison of physical flow characteristics and dimensionless numbers between device inlet setpoints and video analysis pipeline extracted values for 14 repetitions of the same experiment. Experiments were conducted with 1 M $KHCO_3$ and pure CO_2 (Q_L=0.624 ml/min Q_G=1.87 sccm) with no applied current. The average data values are presented ± standard deviation (n=14). ρ=fluid density (kg/m^3), U=two-phase velocity (m/s), d=hydraulic diameter (m), μ=dynamic viscosity (kg/(m·s)), u_B=Bubble velocity (m/s), σ = interfacial tension (N/m), g= standard gravity (9.81 m/s^2)

Parameter	Equation	From Setpoints	From Video Analysis Low Value (outlier)	Average Value	High Value (outlier)
Gas Velocity (mm/s)	N/A	7.5	5.6	7.8 ± 0.3	11.1
Gas Bubble Length (mm)	N/A	N/A	7.9	9.8±0.3	11.6
Reynolds	$Re = \frac{\rho U d}{\mu}$	19.9	10.6	11.5±0.2	11.5
Capillary	$Ca = \frac{\mu u_B}{\sigma}$	1.0*10^{-4}	7.7*10^{-5}	1.1*10^{-4} ±3.8*10^{-6}	1.4*10^{-4}
Froude	$Fr = \frac{U}{\sqrt{gd}}$	0.071	0.038	0.041±0.0007	0.041
Bond	$Bo = \frac{\Delta\rho g d^2}{\sigma}$	0.53			

CO2RR performance single-phase versus multi-phase slug flow

To understand if multiphase flow can bring improvement over using a CO_2-saturated single liquid flow, we first compared these two regimes (Fig. 2a) for a model reaction of CO_2 to carbon monoxide (CO) reduction on a silver mesh cathode; a nickel foam anode, pre-saturated 1 M $KHCO_3$ catholyte, and 1 M KOH as the anolyte were used (Fig. 2b). We carried out electrochemical experiments over the range -2.5 to -50 mA/cm^2 (Fig 2c,d). CO FE peaked at -5 mA/cm^2 for both flow regimes, achieving a maximum of 64±5 % for multi-phase slug flow and only half of this (30±8%) for liquid-phase-only flow. After this peak, CO FE decreased with increasing current density, and the additional current increasingly promoted greater hydrogen evolution (Supplementary Fig. 1a).

At -5 mA/cm^2 and above, slug flow consistently outperformed single-phase liquid flow. The enhancement ratio of partial current density (i_{CO}) comparing slug to liquid flow ranged from 1.7±0.2 to 2.1±0.3. At -50 mA/cm^2, the peak achieved i_{CO} increased from -4.7±0.6 mA/cm^2 in single-phase flow to -7.8±0.9 mA/cm^2 in slug flow.

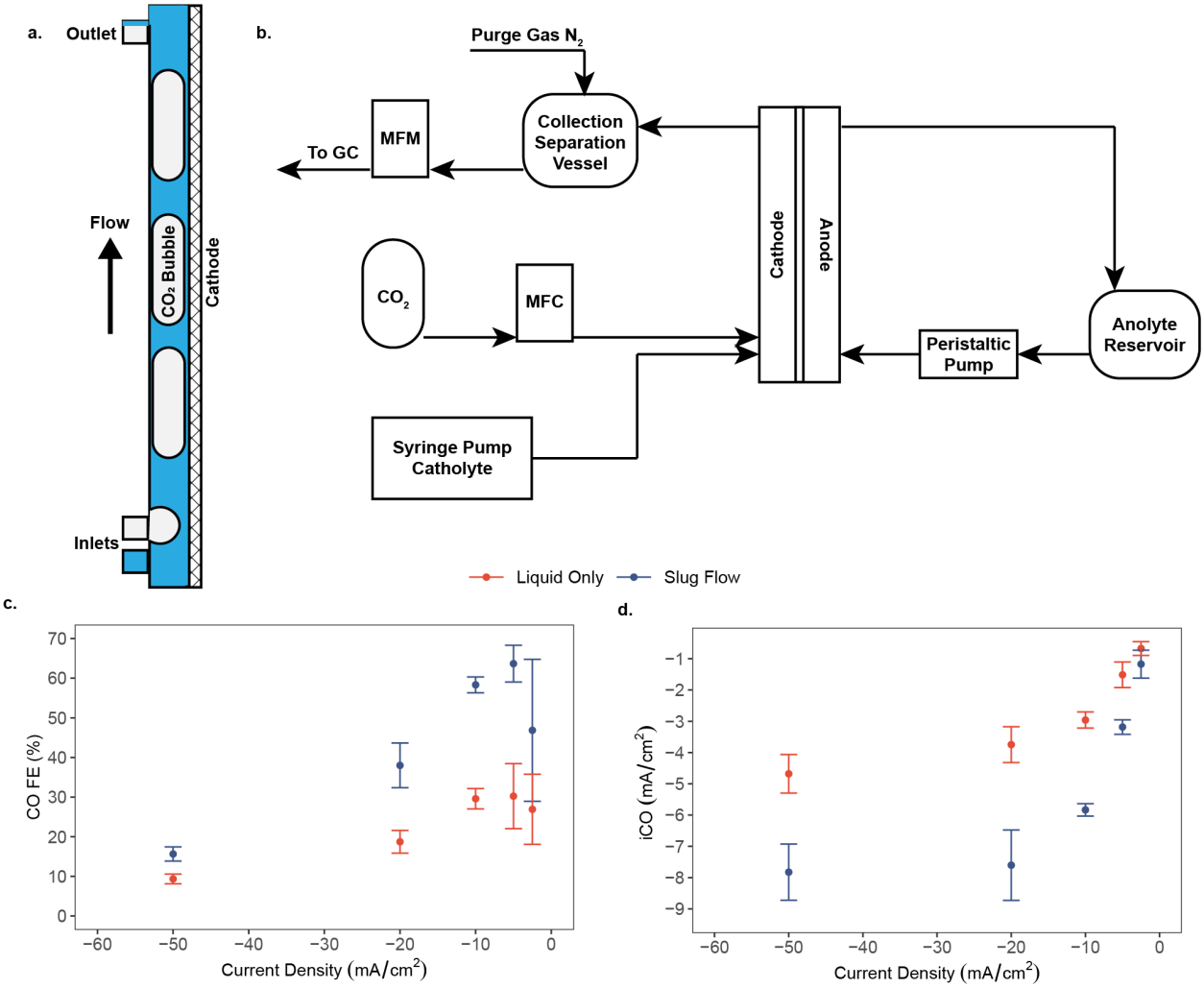


Figure 2: Single-phase versus multi-phase slug flow for electrochemical CO_2 reduction. a, Schematic illustration of Taylor slug flow and its formation in our reactor. **b,** Schematic illustration of the experimental set-up for multi-phase flow operation and product quantification. **c-d,** Performance of the reactor in (**c**) CO FE and (**d**) i_{CO} under either a single-phase liquid-only regime or a multi-phase slug flow regime. The data points are presented as the mean value ± standard deviation (n=3). Voltage ranged from -1.96 to -3.02 V for liquid-only and from -1.86 to -3.03 V for slug flow.

This improvement can be correlated with improved mass-transfer mechanisms introduced by slug flow. The CO_2 gas bubble increases the supply of CO_2 within the reactor and introduces additional mass transfer mechanisms beyond liquid-only flow. The mass transfer pathways come from the previously discussed improvements of slug flow: transfer from the gas bubble caps to the liquid slug, transfer from the slug to the wall (electrode), and transfer from the gas bubble through the thin liquid film to the wall (electrode).

Flow hydrodynamics were altered under applied current (Supplementary Table 1). On average, the bubble velocity and slug length decreased, while bubble length increased. Slug flow was maintained under applied current, but since flow behavior has changed, we related selectivity and i_{CO} to the flow characteristics during operation.

Effect of slug flow characteristics on CO2RR performance

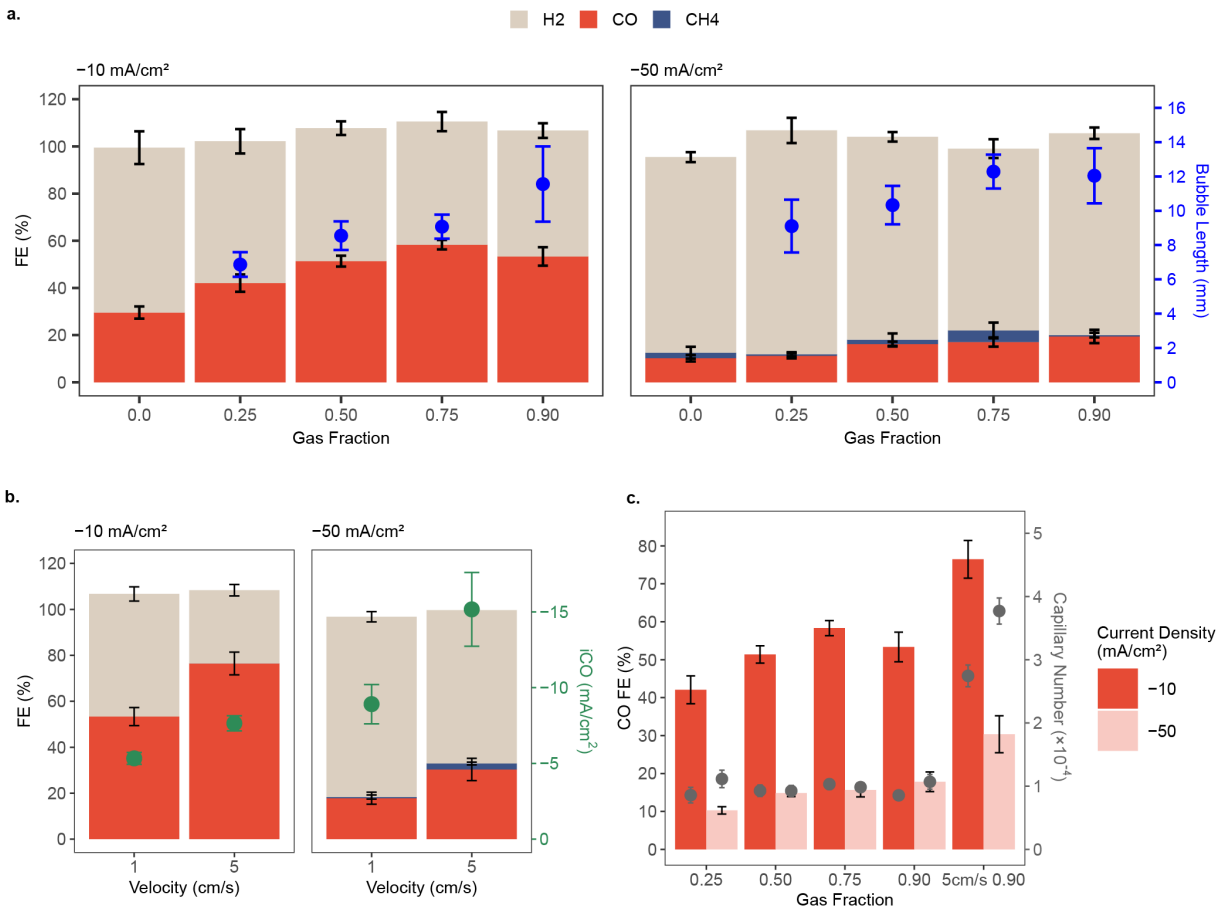


Figure 3: Impact of the slug flow on CO2RR: a, CO FE at various gas flow fractions at both -10 and -50 mA/cm^2 and the corresponding average bubble lengths (n=3). **b,** FE dependence on total flow velocity in slug flow at -10 and -50 mA/cm^2 and the i_{CO} achieved

at each condition (n=3). **c,** CO FE and the corresponding Ca ($*10^{-4}$) for each flow and current condition (n=3).

Since multiphase flow allows us to improve FEs and partial current density as compared to liquid flow only, we sought to further control FEs through achieved flow regimes. We compared liquid-only flow against four gas fractions (0.25,0.5,0.75,0.9) at -10 and -50 mA/cm^2 (Fig. 3a). At -10 mA/cm^2, introducing gas at a G25:L75 ratio increased CO FE from 30±3% to 42±4%. At -50 mA/cm^2, no significant increase appeared until G50:L50, where it increased from 9±1% with liquid only to 15±1%. For both current densities, increasing the gas fraction increased CO FE, although at -10 mA/cm^2, the 0.9 gas fraction does not provide improvement beyond 0.75.

The high-current density tests also produced methane, however, it is unlikely to stem from a different reaction mechanism, and is most likely due to the incorporation of minor copper impurities from the copper tape used for current collection, and we expect the effect of a minor impurity to be more pronounced under a higher current[42]. Given very low FEs (less than 5%), the limitation of methane detection through a gas chromatography system (GC), and the fact that post-reaction gas sampling happens under nitrogen dilution, methane production trends were not analyzed.

We also tested total two-phase velocities of 1 and 5 cm/s at a fixed gas-liquid ratio at both currents (Fig. 3b). Increasing the total velocity increased the CO FE at -10 mA/cm^2 from 53±4% to 77±5%, and at -50 mA/cm^2 from 18±3% to 30±5%. I_{CO} was also increased: at -10mA/cm^2, -5.3±0.4 mA/cm^2 to -7.6 ±0.5 mA/cm^2, at -50 mA/cm^2, -8.9 ±1.3 mA/cm^2 to -15.2 ±2.4 mA/cm^2. The increase in current density indicates that higher velocity further enhances mass transport beyond the limits observed at lower velocities.

We further sought to rationalize this data in the context of Ca number values, which we can calculate using the data extracted from operando tracking. With greater gas fraction, the bubble size increases and liquid slug decreases (Fig. 3c, Supplementary Fig. 2a,b,c & Supplementary Fig. 3), correlating with a higher CO FE. These trends suggest the ratio enhancement arises from geometric flow changes. The longer bubble increases CO_2 supply and film contact, and the shorter slug increases recirculation frequency[25][43][43]. Ca does not significantly change with fraction changes, while increasing velocity increases Ca by ~3-4x. Although vortex location and recirculation both shift with Ca[44][44], these changes are significant at higher Ca ranges than our values, so the recirculation pattern would not significantly change; therefore, enhancement does not result from interfacial changes. Instead, velocity acts through additional convection. The ratio increases the slug renewal frequency, while the velocity increases the renewal rate. Higher velocity also thins the diffusion boundary layer[29]. However, for slug flow, these pathways cannot be separated, so no single dominant mechanism can be extracted for

the ratio effect; hence, we sought to further explore the velocity enhancement mechanism by comparing slug flow with annular flow.

Multi-phase Annular Flow Regime

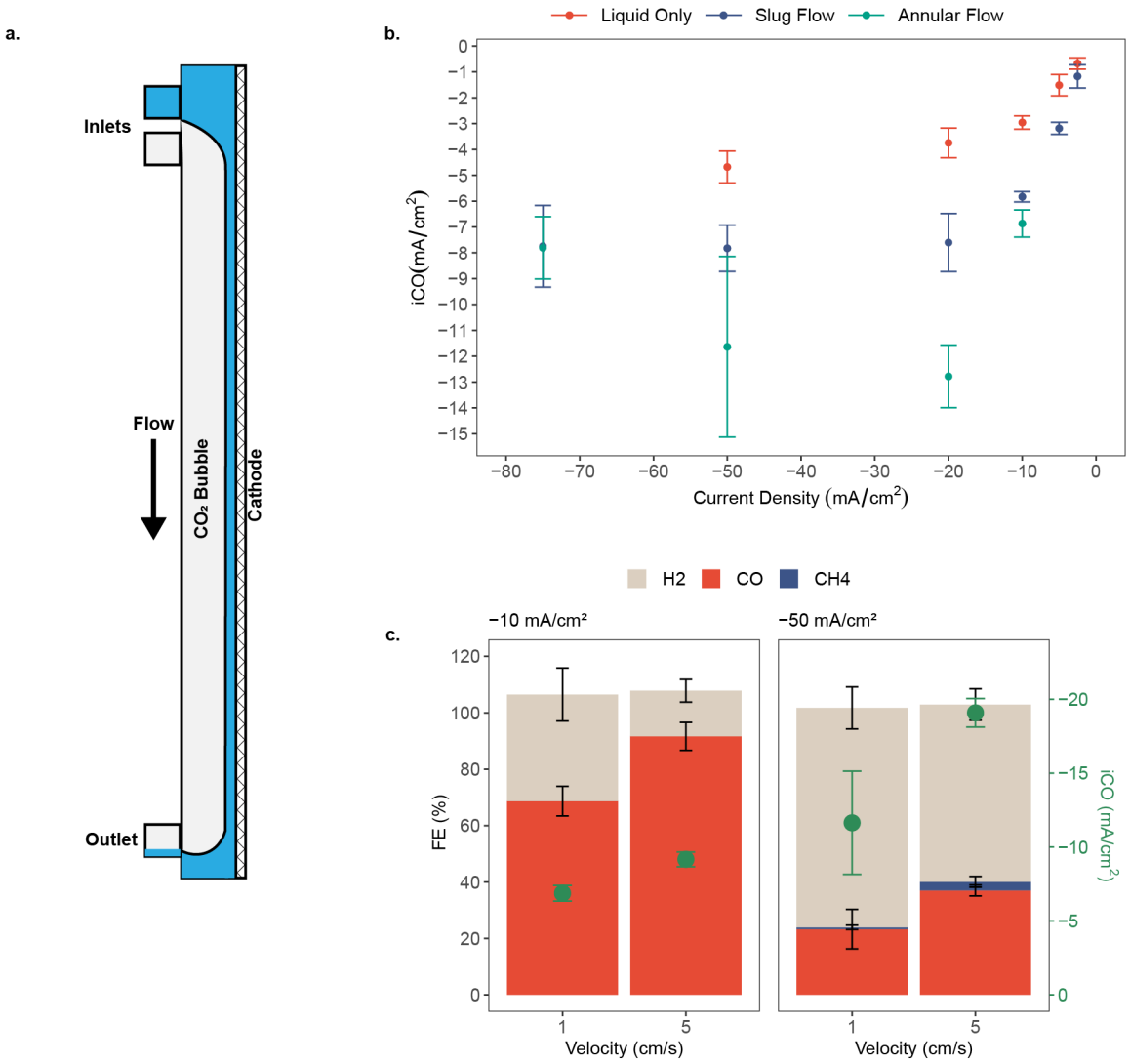


Figure 4: Annular flow reactors for electrochemical CO_2 conversion, Schematic of inverted reactor with the observed annular film flow. **b,** i_{CO} comparison between liquid-only, slug flow, and annular flow regimes over -2.5 to -75 mA/cm^2 (n=3). Gas to liquid ratio is 75:25. **c,** FE dependence on total flow velocity in annular flow at -10 and -50 mA/cm^2 and the i_{CO} achieved at each condition (n=3).

With our low Froude numbers, we know that gravity is playing a role in our system, especially since it has a larger impact on square capillaries and in up-flow conditions[38]. Therefore, we could access a gravity-driven annular film flow regime by reversing the reactor[25] (Fig. 4a). With annular flow, bubble length always equals the length of the channel, so our recording and tracking system is not used.

We compared i_{CO} for annular and slug flow over the range -10 to -75 mA/cm^2 (Fig. 4b). Annular flow further enhances the transport-limited CO partial current density compared with slug flow. At -20 mA/cm^2, i_{CO} reaches -12.8±1.2 mA/cm^2, a 1.7±0.3 times enhancement over slug flow. However, at higher currents, i_{CO} declines back to the magnitude of slug flow: at -75 mA/cm^2, annular flow i_{CO}=-7.8±1.2 mA/cm^2, slug flow i_{CO}=-7.7±1.6 mA/cm^2.

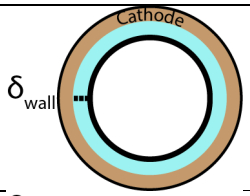
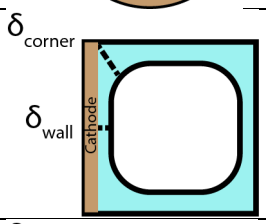
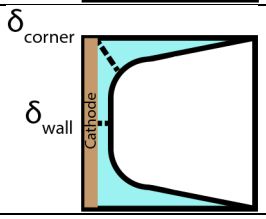
We also investigated how increasing velocity in the inverted annular flow would affect the performance of CO2RR (Fig. 4c). Increasing from 1 cm/s to 5 cm/s, increases CO FE from 69±5% to 92±5% at -10 mA/cm^2 and from 23±7% to 37±2% at -50 mA/cm^2. I_{CO} is also increased: at -10 mA/cm^2 from -6.9±0.5 to -9.2±0.5 mA/cm^2, and at -50 mA/cm^2 from -11.6±3.5 to -18.5±1.0 mA/cm^2.

The presence of a large bubble with only film on the electrode enhances the transport ceiling; however it also likely results in the i_{CO} decrease that we observed at high currents. With a thin film, there is a limited supply of CO_2 that can be delivered across the interface. Once it reaches this peak, the consumption at the electrode surface is outrunning the supply at higher currents and greater amounts of OH^- are generated, which can spike the local pH and collapse the buffering effect provided by the catholyte resulting in lost CO_2 supply to the electrode and conversion to carbonate/bicarbonate[31].

Exploring Velocity Enhancement Mechanism Between Regimes

Our results demonstrate the ability to control the reaction through multiphase flow and achieve CO FE of over 90%, yet the transport ceiling limits operation at current densities over 100 mA cm^{-2}, which are broadly considered necessary for economically viable reactors. To probe the underlying transport mechanisms, we compared film thicknesses predicted from hydrodynamic correlations against calculated effective diffusion length, δ_{eff}, from the limiting currents (Supplementary Note 2). While the correlations provide a theoretical physical thickness, the calculated effective lengths represent lumped transport contributions within a single regime (Table 2)**.** Yet, these can be used for a comparative analysis of the effective diffusion length for both the flow types studied in this paper (Taylor slug and annular in a rectangular channel) and the modeling reference from the literature (Taylor slug in a tubular channel).

Table 2: Correlations of film thickness in different geometries and multi-phase flow regimes and effective diffusion lengths from experimental results**.** All values correspond to -50mA/cm^2 experiments. Ca=Capillary number (-), d=hydraulic diameter (m), i=current density (mA/cm^2), L=length (m), μ=dynamic viscosity (kg/(m·s)), ρ=fluid density (kg/m^3), Q=volumetric flowrate (m^3/s).

Flow Type	Channel Films	Equation	Variables	Diffusion Length (μm)	
				Velocity	
				1 cm/s	5 cm/s
Tubular		Aussillous-Quéré	Ca	2.5	3.0
Rectangular Slug Flow		Wall Film (1-5%)	d_H	20-100	20-100
		Corner Film[25]	Ca	135.6	151.7
		Electrochemical Data Model	i_{HER}, i_{CO},L_B,L_S,u_B	78.3	50.5
Rectangular Annular Flow		Nusselt Film Theory	μ,ρ,Q_L,W	107.1	183.1
		Electrochemical Data Model	i_{HER}, i_{CO},L_B,L_S,u_B	74.6	45.1

In the subsequent analysis, we sought to systematically investigate film formation using different channel geometries. The Aussillous-Quéré correlation is used for tubular Taylor flow reactors and predicts a film of only ~3μm from our Ca, which *Bagemihl*[31] model predicts would greatly boost the performance of CO2RR.

Interestingly, such improvement is not observed experimentally in rectangular channels, and we reviewed different modeling approaches to determine underlying fundamental phenomena. In rectangular channels with low Ca (<0.04), gas bubbles are non-axisymmetric and flatten against the wall, creating a thicker corner film and a thinner wall film[25][45][45][46][46], and the contribution of a thicker film layer around the corners becomes more pronounced. Experimental studies have found the wall film is 1-5% of the channel width (20 -100μm in our channel), significantly greater than the tubular correlation. As an upper bound, we use the corner film correlation of *Kreutzer et. al.,*[25], which yielded a diffusion length of 135-151μm. We then calculated δ_{eff} from our electrochemical data[31]. We utilized the assumption of a stagnant film, where the mass-transfer boundary layer

equals the film thickness ($\delta = \delta_F$), valid if the convective transport is less significant than diffusive transport[30]. For annular flow, Nusselt Film Theory is used to estimate the film thickness, and the gas bubble length was assumed to fill the channel, reducing the model to a simpler Nernstian solution without the slug contributions; δ_{eff} represents the stagnant film layer that reproduces the measured currents, not the physical film thickness.

We found that in slug flow, δ_{eff} is below the corner-film values and within the 1-5% wall-film range. In annular flow, δ_{eff} is smaller than the calculated Nusselt film thickness. The velocity trends for both regimes are opposite when comparing correlations to δ_{eff}. Nusselt theory predicts that the film thickness will increase with velocity, and in slug flow the wall film is independent of Ca. However, δ_{eff} decreases and i_{CO} increases with increasing velocity for both regimes. This indicates that CO_2 delivery is not governed by physical film thickness, but by a thinner concentration boundary layer. Utilizing δ_{eff} in the stagnant film assumption ($e.g. @5\frac{cm}{s}\, slug\ \ \frac{u_B \delta}{D}\frac{\delta}{L_F} \approx 2.91 < 1$) shows that the stagnant film assumption does not hold ($\delta \neq \delta_F$) and that convection has a significant contribution. This indicates that transport is not governed by film thickness but by a decoupled mass-transfer boundary layer that is controlled by convection.

The enhancement arises primarily from thinning and renewal of the diffusion boundary layer rather than from changes in the film thickness. The relevant design levers are frequency and rate renewal, set by slug length and velocity, together with gas-liquid interfacial area, controlled by bubble length, rather than film thinning as in tubular reactors[31]. These levers have only been confirmed on our silver catalyst, however understanding the enhancement in this case provides a powerful tool to study the enhancements on other catalysts with different product distributions and mechanisms.

Towards flexible operation under an intermittent power supply

While the current density achievable in the multiphase reactors remains fundamentally limited in rectangular channels due to corner effects and did not exceed -75 mA/cm^2 in this study, we sought to understand if the proposed flow regimes can fundamentally address the challenges of limited stability in CO2RR. We first further optimized the counter electrode reaction, oxygen evolution (OER), the main contributor to the full-cell voltage. We modified our Ni foam electrode by plating NiFe (Methods section), and interestingly, the effects of catalyst plating were only well pronounced when we co-plated the same catalyst on the walls of the titanium flow field, suggesting that otherwise non-coated titanium could contribute to performance losses (Fig. 5a-c). The combination of a plated flow field and more concentrated electrolyte resulted in a 726.6 ± 131.2 mv decrease for slug flow and a 1120.4 ± 321.3 mV decrease for inverted annular flow at -75

mA/cm^2. These anode-side modifications improved energy efficiency without affecting cathode-side selectivity (Supplementary Fig. 4).

For the most energy-efficient anode configuration, we assessed both the continuous voltage and CO FE stability and the recovery across on/off cycles under an annular flow regime at -75 mA/cm^2 (Fig. 5d). Between operating hours, the reactor was left untouched with both sides filled with bicarbonate to avoid membrane drying; to restart, fresh electrolyte was introduced and flow and current resumed. Over 5 days, the voltage remained stable when applying -75 mA/cm^2, and CO FE also recovered between days with no reconditioning, demonstrating that this reactor can tolerate repeated shutdowns (length of shutdowns varied between 2 – 42 hours). After initial stability testing, the reactor was tested after a 30-day shutdown, during which the full cell voltage increased by approximately 400-500 mV, and CO FE decreased by only 6% (Supplementary Fig. 12). The resilience of this reactor to repeated shutdowns is a key advantage of this multi-phase architecture. It avoids the flooding and precipitation failure modes of GDE and enables a simple restart procedure that allows intermittent renewable-powered operation.

Encouraged by the unprecedented stability under intermittent power supply, and the fact that we can consistently produce syngas with the ratio needed for Fischer-Tropsch synthesis, we performed a TEA analysis to determine whether the proposed reactor can be economically viable despite the lower current densities. We followed a CO2RR TEA protocol[47], assuming PEM membrane use to mitigate loss of CO_2 through formation of bicarbonates, 75 mA/cm^2 current density, 3 V of full cell voltage (details in Methods – TEA). We were interested in how this synthesis scheme could fit into dynamic electricity pricing, and thus we evaluated total syngas production cost as a function of electricity price and hours on stream per year, assuming that the reactor would only operate when electricity is available at low cost. Literature suggests that dynamic pricing can offer electricity at zero or even negative cost during peak hours, yet we adopted a more conservative scenario of looking at prices between \$0.01-0.03/kWh (Fig. 5e). We found that as long as the reactors operate for a minimum of 1000 hours per year (being 1/8 of the typical time for a continuous operation), they can deliver syngas below the current market price of 0.8-1 \$/kg. While multiphase flow reactors do not deliver the same current density as GDEs, the ability to leverage electricity at a much lower cost opens up an interesting economic opportunity.

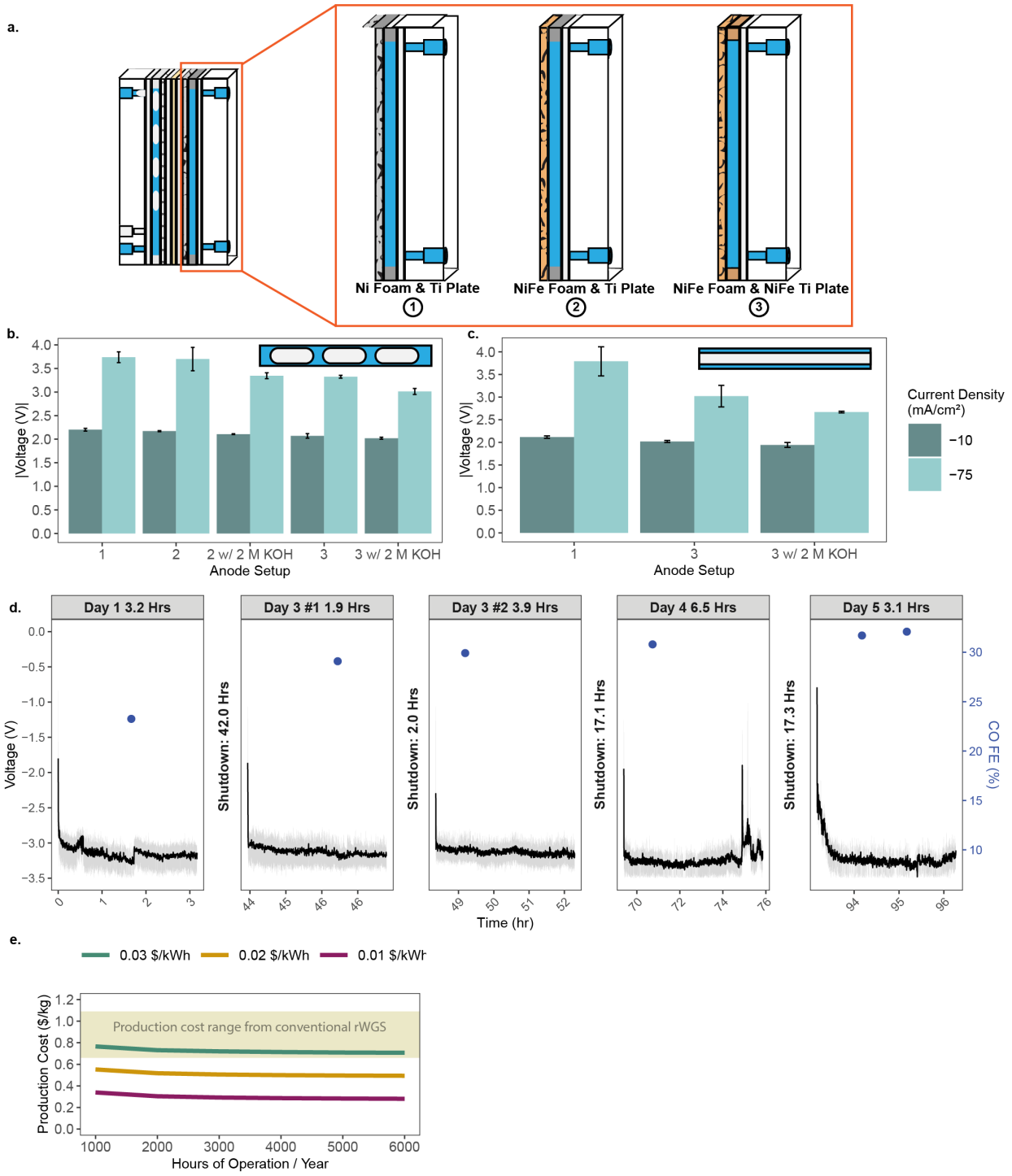


Figure 5: Towards stable performance under intermittent power supply: a, Schematic of anode side optimization changes including (1) base nickel foam and titanium plate, (2) Nickel-iron deposited nickel foam and base titanium plate, and (3) Nickel-iron deposited nickel foam and nickel-iron deposited nickel plate. **b,c** Absolute value of voltage with anode side and anolyte concentration changes under (**b**) slug flow regime (anodes 1,2, and 3) and (**c**) annular flow regime (anodes 1 and 3) at -10 and -75

mA/cm^2 (n=3*)*. **d,** Voltage stability over five days with the measured CO FE at -75 mA/cm^2 under annular flow. The dark black line represents voltage average over 10 seconds, gray shaded area represents voltage range fluctuation with sampling interval of 0.1s. **e,** TEA with dynamic electricity pricing. The yellow shaded box represents the production cost range of the conventional Reverse Water Gas Shift (rWGS) pathway[50].

Conclusion

We demonstrate that multi-phase flow electrochemical reactors offer an important interface to systematically integrate within both fundamental and applied CO2RR studies. By eliminating the GDL, we fundamentally eliminate the problem of flooding and GDL rupture, allowing us to deconvolute catalytic effects from microenvironment degradation, while maintaining improved mass transfer. Regimes that act as a CO_2 transport enhancement mechanism are governed by boundary-layer renewal and not film thickness. By leveraging slug and annular flow, we identified key design levers, velocity, gas fraction/bubble length, and orientation, that improved performance in rectangular channels. Though current density is lower than that of further transport-optimized GDEs, we demonstrated the ability of this reactor to withstand shutdowns and maintain consistent energy and selectivity performance with minimal failure mode engineering necessary. As a result, proposed reactors can leverage low-cost intermittent electricity sources and deliver syngas at a cost lower than current market cost, provided they operate for a minimum of 1000 hours per year. Our findings provide mechanistic insight into multi-phase rectangular-channel silver reactors and the design levers needed to further explore multi-phase flow regimes in electrochemical CO2RR. Moving beyond a single CO2RR catalyst and reaction are clear next steps in exploring multiphase CO2RR; this includes also insights into numbering up channels, changing channel shapes, and exploring beyond ambient conditions, to broadly advance understanding of reaction mechanisms under conditions feasible for future scale-up.

Acknowledgements

We acknowledge the support of the Advanced Research Projects Agency-Energy (ARPA-E), U.S. Department of Energy. The information, data, or work presented herein was funded in part by the Advanced Research Projects Agency-Energy (ARPA-E), U.S. Department of Energy, under Award Number DE-AR0001945. The views and opinions of authors expressed herein do not necessarily state or reflect those of the United States Government or any agency thereof. For more information, contact m.barecka@northeastern.edu. Analysis operando bubble tracking code was developed with assistance from Claude (Anthropic, Opus 5). Parameter selection and validation were performed by the authors.

Conflict of interest

The authors are inventors listed on a non-provisional patent application PCT/US2025/036944 for multiphase flow reactors. MHB is a part of the Advisory board of iScience and Chem Circularity. There are no other conflicts of interest to disclose.

Supplementary information

Supplementary information is available at: TBD.

Methods

Chemicals and materials

Potassium Bicarbonate ($KHCO_3$, 99.7-100.5%) and Sodium Hydroxide (KOH, 85%) were purchased from Fischer Scientific. Nickel (II) Nitrate Hexahydrate ($Ni_2NiO_6•6H_2O$, 99%), Iron (III) Nitrate Nonahydrate ($Fe(NO_3)_3•9H_2O$, 98.0-101.0%), and Silver Gauze (80 Mesh woven from 0.115 dia. wire, 99.9% metals basis) were purchased from Thermo Scientific. Nickel Foam (80-120 PPI, 99.99+%) and PiperION AEM (60 microns, self-supporting) were purchased from FuelCell Store. PiperION AEMs were pretreated and utilized in accordance with the manufacturers recommended protocols. Reactor acrylic and grade 5 titanium plates were purchased from Sendcutsend. Copper tape, Kapton tape, and PVC gasket sheet were purchased from Amazon. All materials were used as received.

Catalyst Preparation

Silver mesh was pretreated before reaction. In a single-cell two-electrode system with 1 M $KHCO_3$, silver mesh (cut to size) was utilized as the working electrode and nickel foam was utilized as the counter electrode. Cyclic voltammetry was performed for 10 cycles

between +2 and -3 V at a scan rate of 50 mv/s (Supplementary Fig. 9). The silver catalyst was then attached to the reactor.

For the creating the NiFe modified anode materials, a solution of 0.003 M $Ni_2NiO_6•6H_2O$ and 0.003 M $Fe(NO_3)_3•9H_2O$ was utilized as the plating electrolyte, and a graphite rod was used as the anode. The titanium plate was prepared for plating by sanding all surfaces. Nickel foam was plated at a current of -60mA and the sanded titanium plate was plated at a current of -180 mA.

Experimental set-up

We designed and constructed a transparent electrochemical cell, inspired by *Bagemihl* PhD thesis. The schematic of our reactor design construction is shown in Fig. 1c. The cathode and anode inlet plates were made using transparent acrylic plates to allow for observation of flow within the reactor. The inlet plates were constructed of two separate acrylic plates: the top plate with ~3.3mm inlet ports for attaching tubing, and the bottom plate with ~2.2 mm for the inlet flow path into the corresponding channel. The top and bottom inlet of each plate are 66 mm apart, with the cathode plate having an additional inlet above the bottom inlet for gas flow. The gas flow inlet is 5 mm above the liquid inlet. The inlet plates are then paired with a gas flow plate: the cathode with an acrylic flow field, and the anode with a titanium flow field. Each flow field is 1.6 mm in height, and has a flow channel of 2.6 mm. The catalyst of both the cathode and anode were attached to its corresponding flow field using copper tape, which was then isolated with Kapton polymer tape. The membrane was placed between the cathode and anode flow fields. A gasket is placed between each of the separate reactor plates for sealing. The reactor is sealed using a torque wrench set to a value of 1.5 N.m.

Electrochemical measurements

The CO_2 reduction experiments were carried out in the assembled reactor controlled by Squidstat Plus potentiostat. The prepared silver catalyst with copper tape current collector served as the cathode and the nickel foam with titanium plate current collector served as the anode in a two-electrode system. Before each experiment, a linear sweep voltammetry was carried out from -0.5 to -3V (Supplementary Fig. 10). During operation, saturated liquid catholyte flow is provided using a syringe pump (NE-300) and the CO_2 gas flow rate was controlled using a mass flow controller (MC_100-SCCM-D/5M). For long-term stability/durability tests, an HPLC pump (Agilent Technologies, 1100) was used instead to control catholyte flow. The anolyte flow rate was controlled using a peristaltic pump and was set at a consistent 20mL/min. The outlet multi-phase flow of the reactor was connected to a sealed collection vessel to separate the gas and liquid phases. This vessel was constantly purged with 10 SCCM of nitrogen and the outlet gas flow from the collection vessel was used for analysis.

Product analysis

The gas output from the collection vessel was analyzed using an Agilent 990 Micro GC system equipped with two columns: CP Molsieve 5 Å and PORAPLOT U. The Faradaic efficiency of gas products was calculated using the formulas:

$$\dot{n}_i = \frac{P}{RT}\dot{V}_{N_2}\frac{y_i}{y_{N_2}}$$

$$FE_i(\%) = \frac{zF\dot{n}_i}{I} * 100$$

where, $\dot{V}_{N_2}$ is the nitrogen purge flow rate (1.67*10^{-4} L/s), y_i and y_{N_2} are the measured GC mole fractions, $\frac{P}{RT}$ evaluated at 298 K, 1 atm, z=2, F is the Faradaic constant (96485 C mol^{-1}) and I is the applied current (A). The constant 10 sccm nitrogen purge was utilized, and an internal standard and the outlet product flow was obtained from the measured GC ratio and converted to molar flow. Example output can be seen in Supplementary Fig. 12.

Video Analysis and Operando Bubble Tracking

During multi-phase slug flow, videos were taken through the transparent acrylic cathode face plate to record liquid slug and gas bubble behavior. Videos were taken both before and after current was applied using a Samsung Galaxy S24. For detailed information on the analysis pipeline refer to Supplementary Note 1. Video frames were annotated with bounding boxes around visible bubbles in the channel. The annotated videos were used as training for an object detection model, YOLOv8n, using the ROBOFLOW service. The YOLO model was then integrated into analysis software for extracting experimental hydrodynamic information. This pipeline began with the YOLO detection assigning an ID to CO_2 bubbles across frames. A calibration was performed on a frame from each video, selecting the center point of four of the reactor screws, which defined a 12x20mm box and created a mm-pixel conversion for each video regardless of if camera position moved between runs. Each video was put through the analysis pipeline and an excel workbook was created for every video that provided a range of output sheets: Experiments sheet (overall data view on the number of bubbles tracked, the average flow structure values with standard deviations), Bubbles sheet (information on each individual confirmed bubble), Rejected sheet (information on any rejected bubbles), and Frames sheet (information of each tracker in every frame of tracked video).

Techno-economic analysis (TEA)

The TEA was performed following the protocol of Barecka et al. Given that the reactor designed in this was work was developed on a small scale and still represents a low Technology Readiness Level (TRL), we took a number of worst-case scenario

assumptions, aiming at rather underestimating than overestimating the economic promise. We assumed targeted syngas production rate at 0.02 kg/s (corresponds to a 100 Nm^3/h unit), 0.06 kg/s of CO_2 input, resulting in 50% CO_2 conversion and 100% CO_2 utilization (PEM membrane and no losses to bicarbonate), and experimentally demonstrated 30% CO FE and 3V of full cell voltage.

The operational cost (Opex) consists of CO_2 cost, electricity cost, water cost, separation cost, and 30% margin to account for labor cost and other cost components which are complex to assess for a low TRL solution. CO_2 is assumed to be available at $30/ton. The flow of CO_2, as well as the flow of products (in $mol/m^2/s$) is calculated from mass balances and the Faradaic Efficiency equation (Table 3 in the excel file attached to the protocol). The reactor size was adjusted to obtain the target product ratio. Subsequently, the total current needed for operation was calculated also based on Faradaic Efficiency formula (cell 65B), and energy input needed for operation equals current times full cell voltage (cell 66B). Another key contributor to energy consumption is the separation of unreacted CO_2 from the syngas stream; we used here a literature reference cost for a membrane separation[48] (0.36 MJ/kg CO_2) and multiplied it by unreacted CO_2 flow (Table 3 in the excel file attached to the protocol). Finally, total Opex was obtained by multiplying the total energy input (reactor and separation) by electricity price ($/MJ) and adding the cost of water (water flow multiplied by $0.00143/kg, cost benchmark was obtained from the same protocol), CO_2 cost and by multiplying all by a factor by 1.3.

The capital costs are governed by the cost of electrolyzers, which was assumed here as $5,000/$m^2$ and is multiplied by reactor area, and subsequently multiplied by 1.3 (balance of the plant) and 1.3 (installation cost). The total cost (in $) is then divided by the time the reactor is actively used for CO2RR over a period of 20 years, and this period differs for all scenarios considered in the paper.

References

[1] International Energy Agency. Global Energy Review 2026 (2026).

[2] Arias, P.A. et al. 2021: Technical Summary. In Climate Change 2021: The Physical Science Basis. Contribution of Working Group I to the Sixth Assessment Report of the Intergovernmental Panel on Climate Change Cambridge University Press, Cambridge, United Kingdom and New York, NY, USA, pp. 33−144 (2021).

[3] Adegoke, K. A., Giwa, S. O., Adegoke, O. R., Maxakato, N. W. Systematic mapping on the evaluation of electrochemical CO2 conversion to fuels/chemicals/value-added products and way forward for breakthroughs in electrocatalysis. Scientific African, 20 (2023).

[4] Nitopi, S., Bertheussen, E., Scott, S. B., Liu, X., Engstfeld, A. K., Horch, S., Seger, B., Stephens, I. E. L., Chan, K., Hahn, C., Nørskov, J. K., Jaramillo, T. F., & Chorkendorff, I. Progress and Perspectives of Electrochemical CO2 Reduction on Copper in Aqueous Electrolyte. Chemical Reviews, 119(12), 7610–7672 (2019).

[5] Burdyny, T., & Smith, W. A. CO2 reduction on gas-diffusion electrodes and why catalytic performance must be assessed at commercially-relevant conditions. Energy & Environmental Science, 12(5), 1442–1453 (2019).

[6] Jouny, M., Luc, W., & Jiao, F. General Techno-Economic Analysis of CO2 Electrolysis Systems. Industrial & Engineering Chemistry Research, 57(6), 2165–2177 (2018).

[7] Barecka, M. H., Ager, J. W., & Lapkin, A. A. Carbon neutral manufacturing via on-site CO2 recycling. *IScience*, *24*(6), 102514 (2021).

[8] Deng, W., Lee, A., Kwon, S. *et al.* Copper-catalysed carbon monoxide electrolysis under dynamic operation. *Nat Catal* 9, 823–833 (2026).

[9] Deng, W., Lee, A., Dai, W. *et al.* Techno-economics of polymer-membrane-based CO_2 electrolysers. *Nat. Rev. Clean Technol.* 1, 255–268 (2025).

[10] Wang, R., Ma, J., Sheng, H. *et al.* Exploiting different electricity markets via highly rate-mismatched modular electrochemical synthesis. *Nat Energy* **9**, 1064–1073 (2024).

[11] Liang, S., Altaf, N., Huang, L., Gao, Y., & Wang, Q. Electrolytic cell design for electrochemical CO2 reduction. Journal of CO2 Utilization, 35, 90–105 (2020)

[12] Ma, W., Xie, S., Liu, T., Fan, Q., Ye, J., Sun, F., Jiang, Z., Zhang, Q., Cheng, J., & Wang, Y. Electrocatalytic reduction of CO2 to ethylene and ethanol through hydrogen-assisted C–C coupling over fluorine-modified copper. *Nature Catalysis*, *3*(6), 478–487 (2020).

[13] Montfort, van, Subramanian, S., Erdem Irtem, Sassenburg, M., Li, M., Kok, J., Joost Middelkoop, & Burdyny, T. An Advanced Guide to Assembly and Operation of CO_2 Electrolyzers. *ACS Energy Letters*, 4156–4161 (2023).

[14] Chang, T., Tan, D., Ozden, A., Wang, X.. Copper-base catalysts for CO_2-to-ethanol electrolysis at industrially relevant current densities. *Chem Catalysis*, 6(8) (2026).
[15] De Mot, B., Ramdin, M., Hereijgers, J., Vlugt, T. J. H., & Breugelmans, T. Direct Water Injection in Catholyte-Free Zero-Gap Carbon Dioxide Electrolyzers. *ChemElectroChem*, *7*(18), 3839–3843 (2020).
[16] Kok, J., Kolobov, N., Sharah, M., Foroozan, A., Angizi, S., Dimitriou, K., Higgins, D., & Burdyny, T. Role of the Copper Microstructure on Ethylene Stability during CO_2 Electrolysis. *ACS Energy Letters* (2026).
[17] Kok, J., Albertini, P.P., Leemans, J. *et al.* Overcoming copper stability challenges in CO_2 electrolysis. *Nat Rev Mater* 10, 550–563 (2025).
[18] Albertini, P.P., Toleukhanova, S., Vavra, J.,Louiudice, A., Tileli, V., Buonsanti, R. Oxides and carbonates accelerate copper instability in CO_2 Electroreduction. *J Am Chem Soc.* 148(9), 9784-9792 (2026).
[19] Hao, S., Elgazzar, A., Ravi, N. *et al.* Improving the operational stability of electrochemical CO_2 reduction reaction via salt precipitation understanding and management. *Nat Energy* 10**,** 266–277 (2025).
[20] Kim, J.Y.‘., Zhu, P., Chen, FY. *et al.* Recovering carbon losses in CO_2 electrolysis using a solid electrolyte reactor. *Nat Catal* 5, 288–299 (2022).
[21] O’Brien, C., McLaughlin, D., Böhm, T. *et al.* Scalability and stability in CO2 reduction via tomography-guided system design. *Joule*, 8, 2903-2919 (2024)
[22] Farsi, A., Batta, V., Chan, J.K.D., Miao, R.K, Sarma, P.V., Sinton, D., Bazylak,A. Managing Alkaline CO_2 Electrolyzer Flooding using a Grooved Cathode Gas Diffusion Electrode. *ACS Appl. Energy Mater.* 14 9 (17), 11179–11191 (2026).
[23] Yue, J., Chen, G., Yuan, Q., Luo, L., & Gonthier, Y. (2007). Hydrodynamics and mass transfer characteristics in gas–liquid flow through a rectangular microchannel. *Chemical Engineering Science*, *62*(7), 2096–2108 (2007).
[24] Angeli, P., & Gavriilidis, A. Hydrodynamics of Taylor flow in small channels: A Review. *Proceedings of the Institution of Mechanical Engineers, Part C: Journal of Mechanical Engineering Science*, *222*(5), 737–751 (2008).
[25] Kreutzer, M. T., Kapteijn, F., Moulijn, J. A., & Heiszwolf, J. J. Multiphase monolith reactors: Chemical reaction engineering of segmented flow in microchannels. *Chemical Engineering Science*, *60*(22), 5895–5916 (2005).
[26] Cao, Y., Soares, C., Natan Padoin, & Noël, T. (2021). Gas bubbles have controversial effects on Taylor flow electrochemistry. *Chemical Engineering Journal*, *406*, 126811–126811 (2021).
[27] Horvath, C., Solomon, B. A., & Engasser, J.-M. Measurement of Radial Transport in Slug Flow Using Enzyme Tubes. *Industrial & Engineering Chemistry Fundamentals*, *12*(4), 431–439 (1973).

[28] Nakano, M., Nishiyama, Y., Tanimoto, H., Morimoto, T., & Kakiuchi, K. Remarkable Improvement of Organic Photoreaction Efficiency in the Flow Microreactor by the Slug Flow Condition Using Water. *Organic Process Research & Development*, *20*(9), 1626–1632 (2016).

[29] Zhang, F., Chen, C., Tang, Y., & Cheng, Z. CO2 reduction in a microchannel electrochemical reactor with gas-liquid segmented flow. *Chemical Engineering Journal*, *392*, 124798 (2020).

[30] Zhang, F., Jin, Z., Chen, C., Tang, Y., Mahyoub, S. A., Yan, S., & Cheng, Z. Electrochemical Conversion of CO_2 to CO into a Microchannel Reactor System in the Case of Aqueous Electrolyte. *Industrial & Engineering Chemistry Research*, *59*(13), 5664–5674 (2020).

[31] Bagemihl, I., Bhatraju, C., van Ommen, J. R., & van Steijn, V. Electrochemical Reduction of CO_2 in Tubular Flow Cells under Gas–Liquid Taylor Flow. *ACS Sustainable Chemistry & Engineering*, *10*(38), 12580–12587 (2022)

[32] Bagemihl, I. Insights from operating under gas-liquid Taylor flow and techno-economic optimisation: Reactor design and economics of CO2 electrolysers. [Dissertation (TU Delft), Delft University of Technology] (2024).

[33] Zhou, Y., Ji B., Zhao C., Bo. H., Zhang, Y., Li, H. Role of bubble dynamics in heat and mass transfer in annular flows. *International Journal of Thermal Sciences*, Volume 191, 108348 (2023).

[34] Yin, Y., CZhu, C., Guo, R., Fu T., Ma, Y. Gas-liquid two-phase flow in a square microchannel with chemical mass transfer: Flow pattern, void fraction and frictional pressure drop. *International Journal of Heat and Mass Transfer*, Volume 127, Part B, Pages 484-496 (2018).

[35] Sobieszuk, P., Wawrzyńczak, K. Investigations of mass transfer in annular gas-liquid flow in a microreactor. *Chemical and Process Engineering*, 37. 55-64 (2016).

[36] Zhang, J., Luo, X., Ding, Y., Chang, L., Dong, C. Effect of bipolar-plates design on corrosion, mass and heat transfer in proton-exchange membrane fuel cells and water electrolyzers: A review. *International Journal of Minerals, Metallurgy and Materials.* 31, 1599-1616 (2024).

[37] Luo, X., Ren, C., Song, J., Luo, H., Xiao, K., *et al.* Design and fabrication of bipolar plates for PEM water electrolyzer. *Journal of Materials science and Technology,* 146, 19-41 (2023).

[38] Gupta, R., Fletcher, D.F., Haynes, B.S. Taylor Flow in Microchannels: A Review of Experimental and Computational Work. *The Journal of Computational Multiphase Flows*. 2(1):1-31 (2010).

[39] Etminan, A. Muzychka, Y.S. Pope, K. A Review on the Hydrodynamics of Taylor Flow in Microchannels: Experimental and Computational Studies. *Processes 9*, 870 (2021).

[40] Edvinsson, R.K.,Irandoust, S. Finite-element analysis of Taylor flow. *AIChE J.,* 42: 1815-1823 (1996).

[41] Hazel, A.L., Heil,M. The steady propagation of a semi-infinite bubble into a tube of elliptical or rectangular cross-section. *Journal of Fluid Mechanics*. 470:91-114 (2002).

[42] Chaoqun, M., Haun, F., Dattila, F., Tang, W., *et al.* Origin of unexpected products from CO_2 electroreduction on silver: The role of ppb-level copper impurities in the electrolyte, *ACS Electrochem*, 2(8), 1795-1806 (2026).

[43] Yang, Y., Shi, Y.,Qi, Y., Yao, C. The scaling-up effect on the concentration field and mass transfer of gas–liquid Taylor flow in micro/mini-channel reactors, *Chemical Engineering Science*,Volume 303, 120969 (2025).

[44] Thulasidas, T.C., Abraham, M.A., Cerro, R.L. Flow patterns in liquid slugs during bubble-train flow inside capillaries, *Chemical Engineering Science*, Volume 52, Issue 17, Pages 2947-2962 (1997).

[45] Kolb, W.B., Cerro, R.L. Coating the inside of a capillary of square cross section, Chemical Engineering Science,Volume 46, Issue 9, Pages 2181-2195 (1991).

[46] Fries, D.M., Trachsel F., von Rohr, P.R. Segmented gas–liquid flow characterization in rectangular microchannels. *International Journal of Multiphase Flow*, Volume 34, Issue 12, Pages 1108-1118 (2008).

[47] Barecka, M., Ager, J., Lapkin, A.A. Techno-economic assessment of emerging CO_2 electrolysis technologies. *STAR Protocols,* Volume 2, Issue 4 (2021).

[48] Berstad, D., Nekså, P., Gjøvåg, G. A. Low-temperature syngas separation and CO2 capture for enhanced efficiency of IGCC power plants. *Energy Procedia* 4**,** 1260–1267 (2011).

[49] da Cunha, S.C., Resasco, J. Insights from techno-economic analysis can guide the design of low-temperature CO_2 electrolyzers toward industrial scaleup. *ACS Energy Letters,* 9 (11): 5550-5561 (2024).

[50] Moreno-Gonzales, M., Berger, A., Borsboom-Hanson, T., Mérida, W. Carbon-neutral fuels and chemicals: Economic analysis of renewable syngas pathways via CO_2 electrolysis. *Energy Conversion and Management*, 244 (2021).

Supplementary Files

This is a list of supplementary files associated with this preprint. Click to download.

- SIGDLfreemultiphasereactorsMoranandBareckav1.pdf
- BubbleTrackingExampleOutput.mp4